Supplementary Information

Effects of fluorophore attachment on protein conformation and dynamics studied by spFRET and NMR

Carolina Sanchez-Rico*, Lena Voith von Voithenberg*, Lisa Warner

Don C. Lamb, Michael Sattler

Supplementary Methods

Protein Labeling. Attachment of fluorophores to U2AF65(RRM1,2) constructs was performed using sulfhydryl-maleimide coupling. Single cysteine mutants and the double mutants RRM1,2-C187-C318 and RRM1,2-C187-C326 were reduced in phosphate buffer (20 mM NaH_2PO_4, 20 mM Na_2HPO_4 (or 20 mM KH_2PO_4/20 mM K_2HPO_4), 50 mM NaCl, pH 6.5) containing 1-10 mM DTT. After complete removal of the reducing agent, the labeling reaction was performed by the addition 2-3 molar excess of fluorophore-maleimide conjugates (Atto532-Maleimide, Atto647N-Maleimide, Alexa647-Maleimide, Cy5-Maleimide, Atto565-Maleimide) in buffer (20 mM NaH_2PO_4, 20 mM Na_2HPO_4 (or 20 mM KH_2PO_4/20 mM K_2HPO_4), 50 mM NaCl, 50 µM TCEP, deprived of oxygen, pH 6.8) at room temperature for two hours. The attachment of fluorophores to the protein was confirmed on a denaturing polyacrylamide gel by UV-excitation. Unbound fluorophores were removed by a size-dependent filtration with buffer (20 mM NaH_2PO_4, 20 mM Na_2HPO_4 (or 20 mM KH_2PO_4/20 mM K_2HPO_4), 50 mM NaCl, 0-1mM DTT, pH 6.5). The labeling efficiency was determined from the absorption for the each of the fluorophores and the protein concentration determined photometrically by a bicinchoninic acid assay. Fluorescence correlation spectroscopy (FCS) measurements validated the labeling and removal of unbound fluorophores.

The labeling reactions for NMR experiments were performed in 1 M Tris, 50 mM NaCl, pH 7.5, the removal of unbound fluorophores was done as above in 20 mM phosphate buffer, 50 mM NaCl, 1 mM DTT, pH 6.5.

Solution-based single-molecule FRET measurements. Single-molecule FRET measurements were performed on a custom-build confocal microscope with multiparameter detection and pulsed interleaved excitation [26]. Fluorescently labeled proteins were diluted to concentrations in the tens of picomolar range in phosphate buffer (20 mM KH_2PO_4, 20 mM K_2HPO_4, 50 mM NaCl, pH 6.5) to ensure detection of individual molecules (1-5 fluorescent bursts per second). The fluorophores were excited alternatingly by pulsed 532 nm (PicoTA 530 Picoquant, Berlin, Germany) and 640 nm lasers (LDH-D-C640, Picoquant, Berlin, Germany) at a repetition rate of 26.66 MHz and a laser power of 100 µW for both wavelengths (measured at the entrance point of the beam into the objective). Fluorescence was collected by a 60x water immersion objective (Plan Apo IR 60x/1.27 WI, Nikon, Düsseldorf, Germany) and focused onto a pinhole with diameter d=75 µm. A polarizing beam-splitter split the fluorescence according to polarization (PBS3, Thorlabs, Dachau, Germany). The green fluorescence was

then reflected and the red fluorescence was transmitted by a dichroic mirror (640DCXR, AHF Analysentechnik, Tübingen, Germany). After passing an emission filter (Brightline HQ582/75 and HQ700/75 for green and red photons respectively, AHF Analysentechnik, Tübingen, Germany) the signals were detected on four single photon counting avalanche photodiodes (Perkin Elmer, Hamburg, Germany).

For the fluorophore combinations Atto565/Atto647N and Atto565/Alexa647, a similar confocal microscope was used with the laser excitation lines 565 nm (LDH-D-TA-560) and 641 nm (LDH-D-C-640) (Picoquant, Berlin, Germany). Fluorescence was separated by a polychroic mirror (zt405/488/561/633) and filtered by the emission filters for red (ET670/30) and green (ET607/36) (AHF Analysentechnik, Tübingen, Germany).

The data was recording using time-correlated single photon counting cards (SPC-154, Becker and Hickl, Berlin, Germany) and data analysis was performed with a custom written Matlab program (The MathWorks, Ismaning, Germany). The FRET efficiency was determined as a corrected value:

$$E=\frac{F_{\mathrm{DA}}-\alpha F_{\mathrm{AA}}-\beta F_{\mathrm{DD}}}{F_{\mathrm{DA}}-\alpha F_{\mathrm{AA}}-\beta F_{\mathrm{DD}}+\gamma F_{\mathrm{DD}}} \qquad \text{Eqn. 1}$$

with the correction factors α for direct excitation,

$$\alpha = \frac{F_{\mathrm{DA}}^{\mathrm{A}(0)}}{F_{\mathrm{AA}}^{\mathrm{A}(0)}} \qquad \text{Eqn. 2}$$

β for crosstalk,

$$\beta = \frac{F_{\mathrm{DA}}^{\mathrm{D}(0)}}{F_{\mathrm{DD}}^{\mathrm{D}(0)}} \qquad \text{Eqn. 3}$$

and γ for the correction of the relative detection efficiency and crosstalk.

$$\gamma = \frac{\Phi_{\mathrm{A}}\eta_{\mathrm{A}}^{\lambda_{\mathrm{emA}}}}{\Phi_{\mathrm{D}}\eta_{\mathrm{D}}^{\lambda_{\mathrm{emD}}}} \qquad \text{Eqn. 4}$$

Correspondingly, the corrected stoichiometry is defined as:

$$S=\frac{F_{\mathrm{DA}}-\alpha F_{\mathrm{AA}}-\beta F_{\mathrm{DD}}+\gamma F_{\mathrm{DD}}}{F_{\mathrm{DA}}-\alpha F_{\mathrm{AA}}-\beta F_{\mathrm{DD}}+\gamma F_{\mathrm{DD}}+F_{\mathrm{AA}}} \qquad \text{Eqn. 5}$$

Single-molecule FRET measurements of immobilized molecules. Single-molecule FRET measurements were performed on a custom-build prism-type total internal reflection microscope. Measurements were performed by encapsulation of the protein complex in lipid vesicles. Lipids were prepared as described [45] and 400 nM of U2AF65 and 5 µM U9 or 20 µM U4A8U4 were incubated in a hydrating buffer (20 mM KH_2PO_4, 20 mM K_2HPO_4, 50

mM NaCl, pH 6.5) with the lipids. Liposomes with a diameter of 200 nm were prepared by extrusion [45]. A small percentage of the lipids (3%) were labeled with biotin and these lipids were used to immobilize the vesicles to the surface using a biotin-streptavidin-biotin linkage on the surface of quartz prisms [46]. The quartz prism was designed as part of the sample chamber and used to create an angle of total internal reflection for the excitation light [46]. Excitation of the fluorophores was achieved by illumination of the prism by a diode-pumped solid state laser (Cobolt Samba 100, 532 nm, Solna, Sweden) and a helium-neon laser (Polytec Laser 640 nm, München, Germany). An acousto-optical tunable filter (AOTFnC.400-650-PV-TN, Pegasus Optik) was used for switching and intensity regulation of the lasers, which were then combined in a single-mode polarization maintaining fiber. Fluorescence of the sample was collected by a water immersion objective (CFI Plan Apochromat 60xWI, NA 1.2, Nikon, Düsseldorf, Germany) and separated by a dichroic mirror (630DCXR, AHF, Analysentechnik, Düsseldorf, Germany). After passing the emission filters HQ550/88 or HQ715/150 (AHF, Analysentechnik) respectively, the fluorescence of the donor and acceptor fluorophores was detected on two different regions of an EMCCD camera (Andor iXON, Andor Technology, Belfast, Great Britain).

Supplementary Tables

Supplementary Table 1: **Properties of donor and acceptor fluorophores.**

Fluorophore	**Extinction coefficient [1/(M*cm)]**	**Fluorescence quantum yield [%]**	**Fluorescence lifetime [ns]**	**Charge**	
Atto532	115000	90	3.8	-1	
Atto565	120000	90	3.9	+1	hydrophobic
Atto647N	150000	65	3.5	+1	hydrophobic
Alexa647	239000	33	1.0	-3	
Cy5	250000	30	0.9	+1	cis/trans isomerization

Supplementary Table 2: **Förster radii determined for each combination of donor and acceptor fluorophores.**

Förster radius [Å]	Atto647N	Alexa647	Cy5
Atto532	57.2	61.8	63.2
Atto565	62.8	68.3	69.2

Supplementary Figures

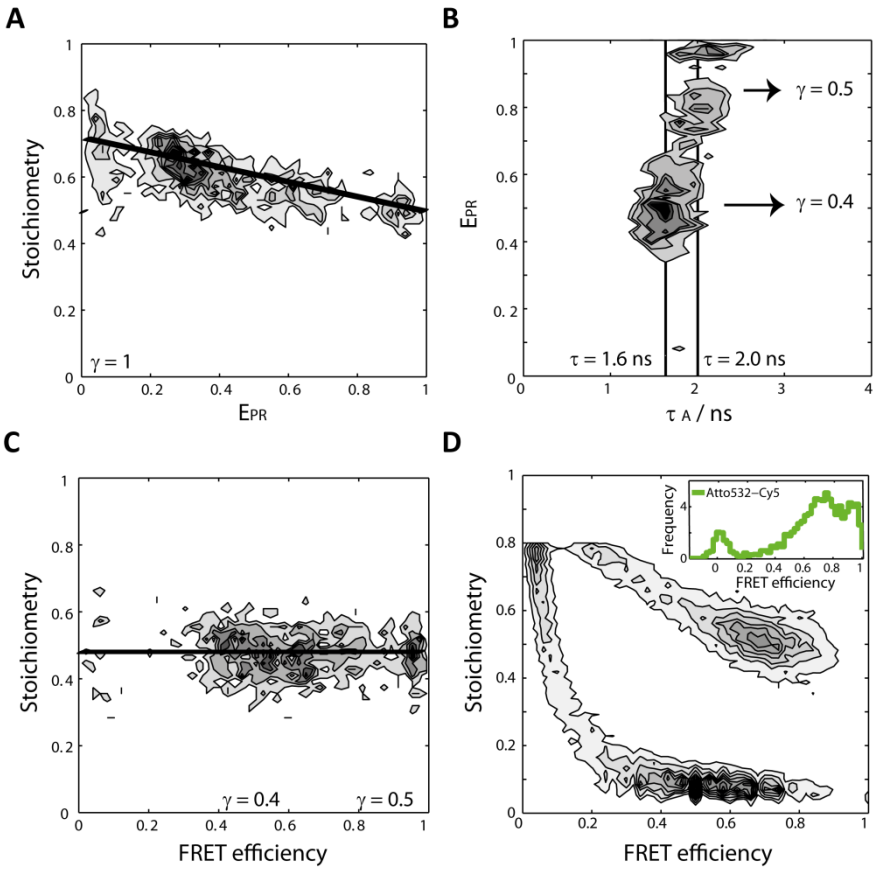

Supplementary Figure S1: **The influence of photophysical effects such as quenching, blinking, and isomerization of cyanine-based acceptor fluorophores on spFRET data.** The data was obtained from spFRET MFD experiments of U2AF65(RRM1,2-C187-C318). (**A**) Histogram of proximity ratio versus stoichiometry for the data of RRM1,2 labeled with Atto532/Alexa647 not corrected for relative detection efficiency (i.e. γ=1, Eqn. 4). The black line is a guide to the eye for the stoichiometry values. (**B**) Histogram of the proximity ratio as a function of acceptor lifetime for the data in (A). The two populations show a different acceptor lifetime and thus need to be corrected by different γ values. (**C**) Corrected FRET efficiency versus stoichiometry histogram from (A). The given γ-factors were applied to individual populations to correct for the differences in acceptor lifetime. The black line serves as a guide to the eye. (**D**) Histogram of FRET efficiency versus stoichiometry for a measurement of U2AF65 labeled with Atto532 and Cy5 in the absence of RNA. Isomerization between two acceptor states is visible as a trailing between a double-labeled and single labeled population. The FRET efficiency histogram of U2AF65 is plotted as an inset.

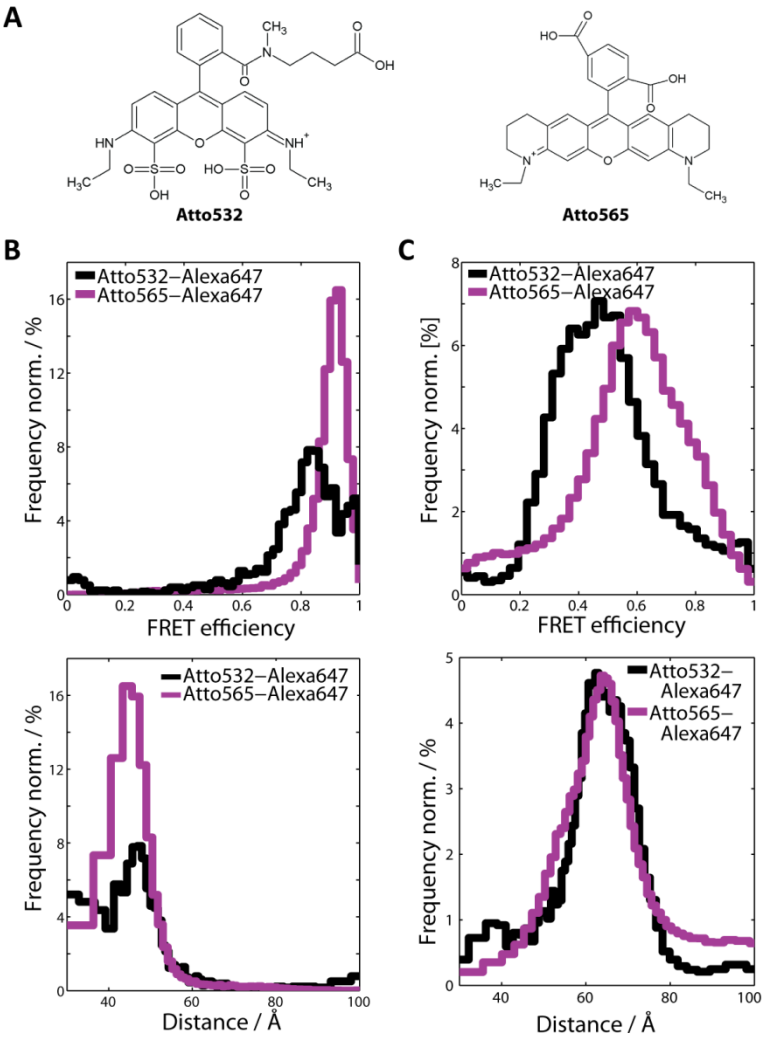

Supplementary Figure S2: **The effect of the donor fluorophore on the conformation of U2AF65(RRM1,2-C187-C318).** (**A**) Molecular structure of the donor fluorophores Atto532 and Atto565 under comparison. FRET efficiency histograms (*upper panels*) and distance distributions (*lower panels*) of RRM1,2 labeled with Atto532 (black) or Atto565 (magenta) and Alexa647 in its free form (**B**) and when bound to RNA (**C**).

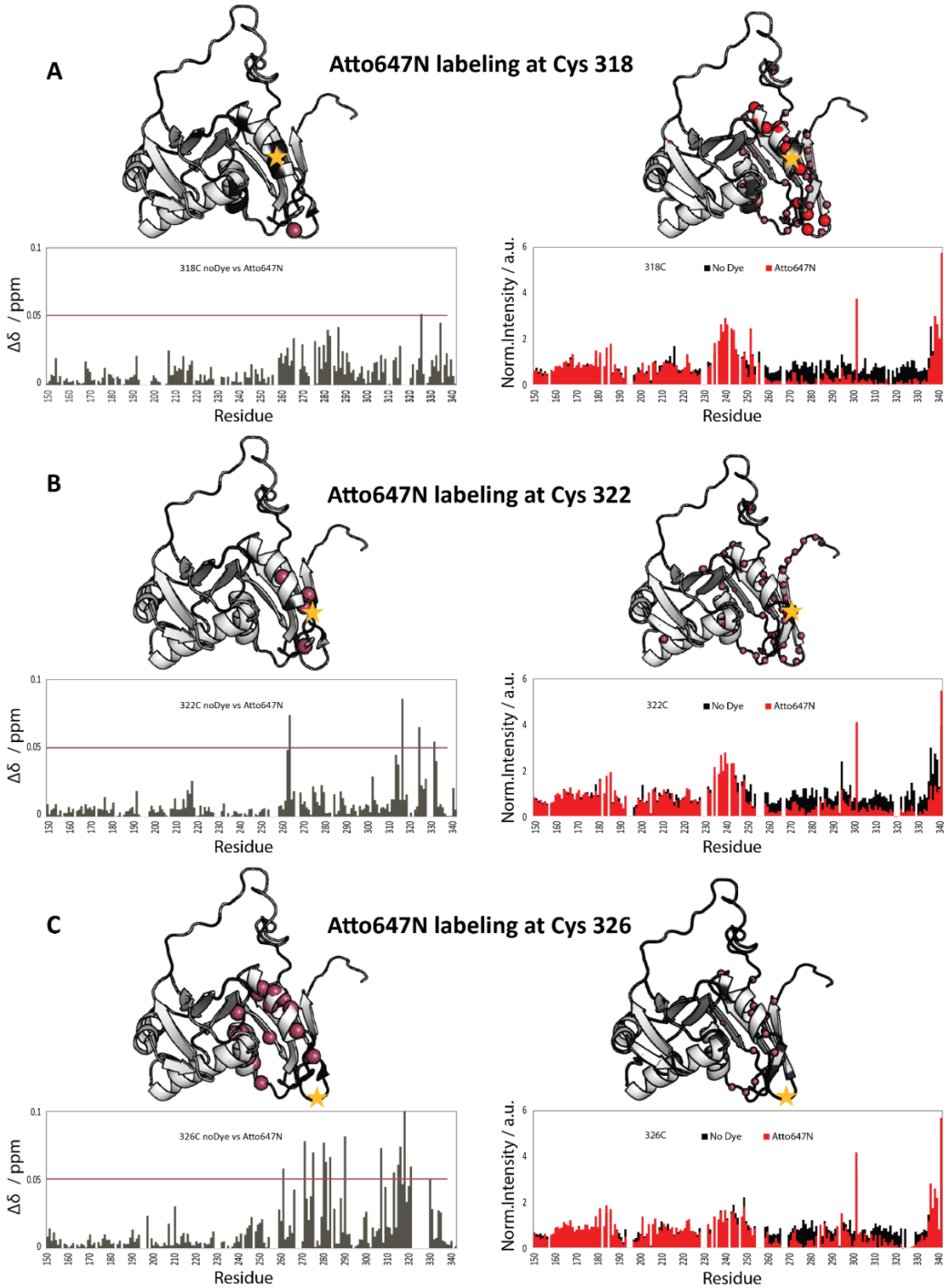

Supplementary Figure S3: **Effects of fluorophore conjugation site on the protein.** Changes in chemical shifts and signal intensities are shown for different attachment sites of Atto647N (yellow star) to U2AF65 RRM1,2, plotted as a function of residue in the lower panels. *Left*: The change in chemical shift is plotted. The pink spheres in the structure indicate residues with chemical shift changes >0.5 ppm. *Right*: The signal intensity as a function of residue. The red spheres in the structure indicate residues with >90% reduction in intensity upon fluorophore labeling and the pink spheres represent the residues with a loss between 90-50%. Data show the NMR analysis of U2AF65 RRM1,2 labeled with Atto647N at residue (**A**) C318, (**B**) C322 and (**C**) C326.

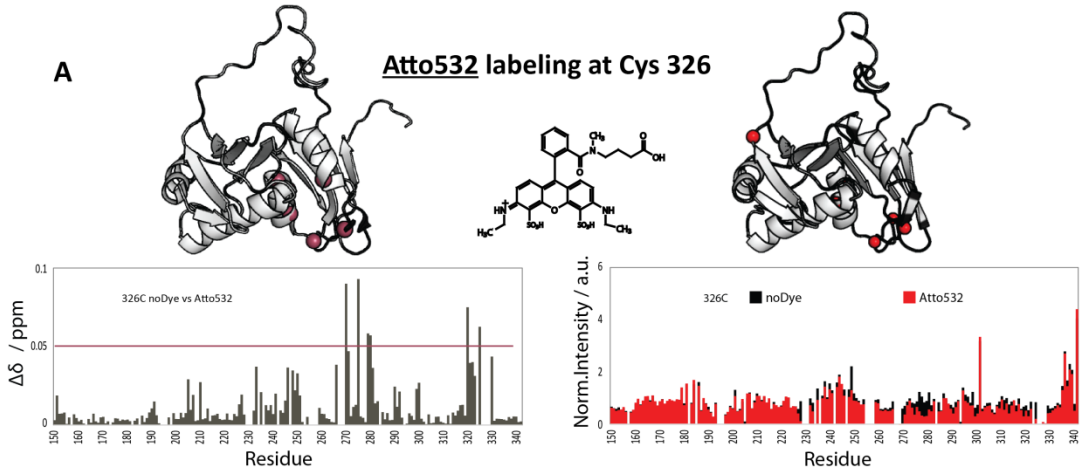
A
Atto532 labeling at Cys 326
326C noDye vs Atto532
Δδ / ppm
Residue
326C
noDye
Atto532
Norm.Intensity / a.u.
Residue

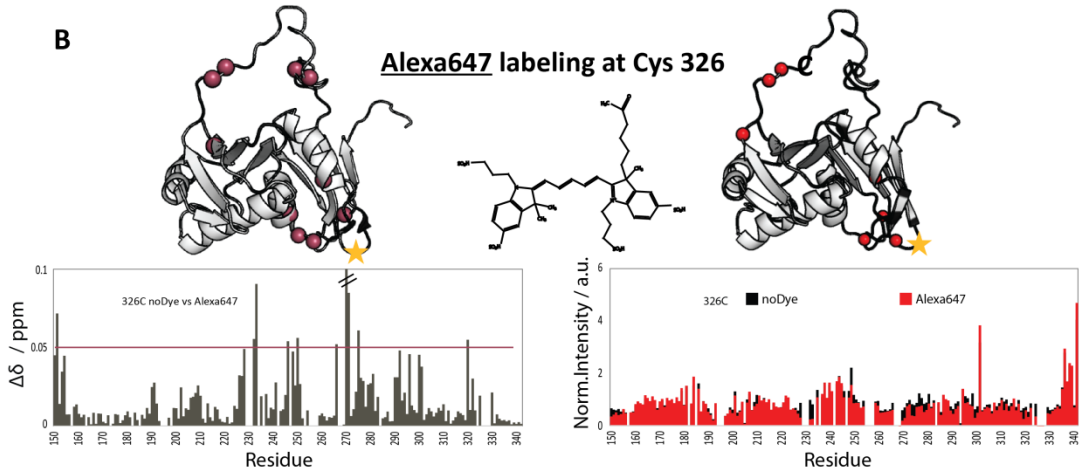
B
Alexa647 labeling at Cys 326
326C noDye vs Alexa647
Δδ / ppm
Residue
326C
noDye
Alexa647
Norm.Intensity / a.u.
Residue

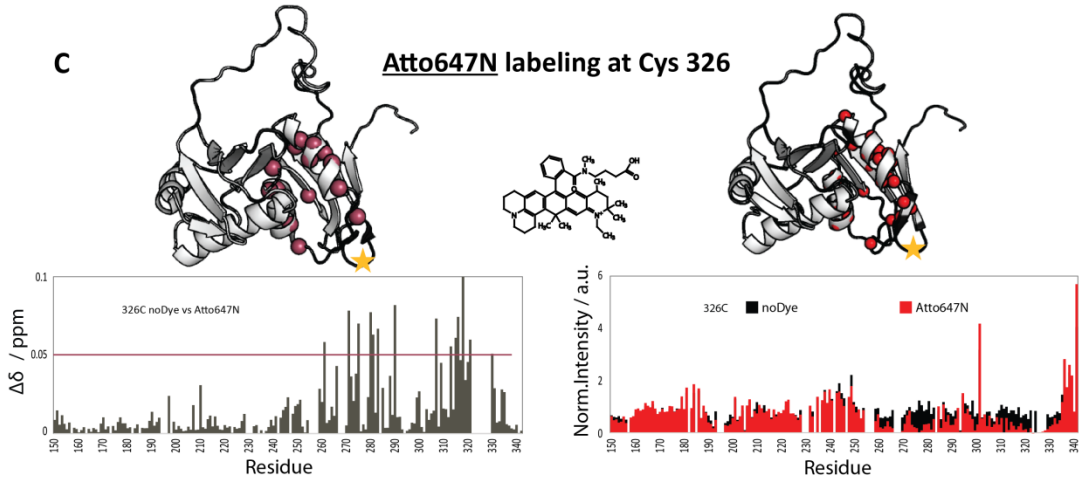
C
Atto647N labeling at Cys 326
326C noDye vs Atto647N
Δδ / ppm
Residue
326C
noDye
Atto647N
Norm.Intensity / a.u.
Residue

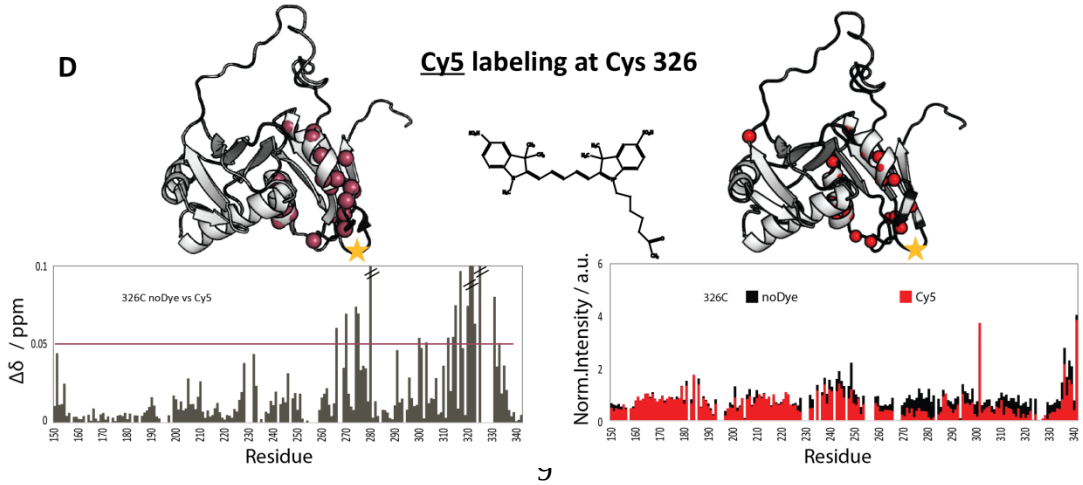
D
Cy5 labeling at Cys 326
326C noDye vs Cy5
Δδ / ppm
Residue
326C
noDye
Cy5
Norm.Intensity / a.u.
Residue

Supplementary Figure S4**: Effect of dyes with different chemical features attached at position 326** (yellow star)**.** Changes in chemical shifts and signal intensities of U2AF65 C326-RRM1,2 are shown for the unlabeled protein vs protein labeled with the fluorophores: (**A**) Atto532, (**B**) Alexa647, (**C**) Atto647N and (**D**) Cy5. On the *left* side, the chemical shift is plotted as a function of residue and pink spheres on the structure indicate the residues with changes larger than 0.5 ppm. On the *right* side, the signal intensity is plotted as a function of residue. Red spheres in the structure indicate residues with loss of more than 60% of peak height upon fluorophore labeling.

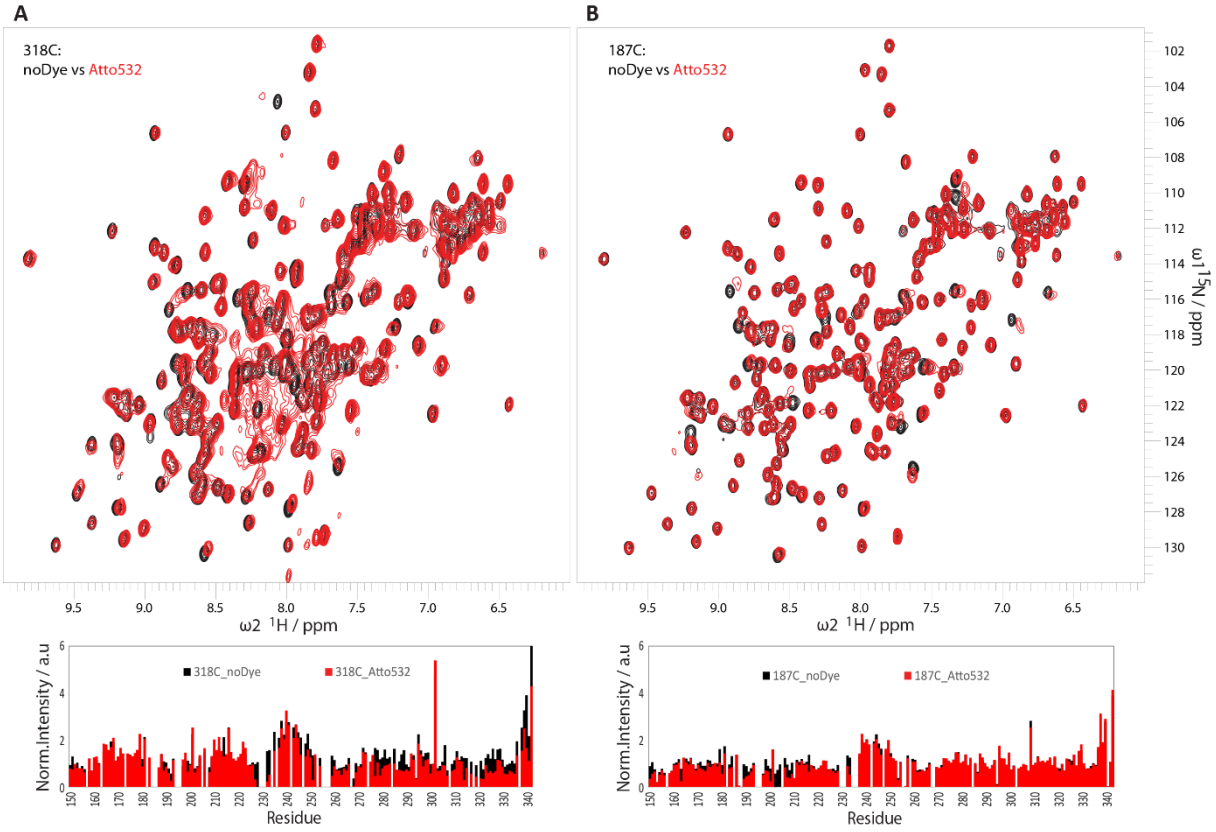

Supplementary Figure S5: **The effect of the donor fluorophore Atto532 at positions C318 and C187 on the conformation of U2AF65 (RRM1,2) studied by NMR.** Comparison of the $^{1}H,^{15}N$-HSQC spectra and intensity vs residue plots of unlabeled RRM1,2 (black) and Atto532-labeled RRM1,2 (red) at the positions (**A**) C318 and (**B**) C187.

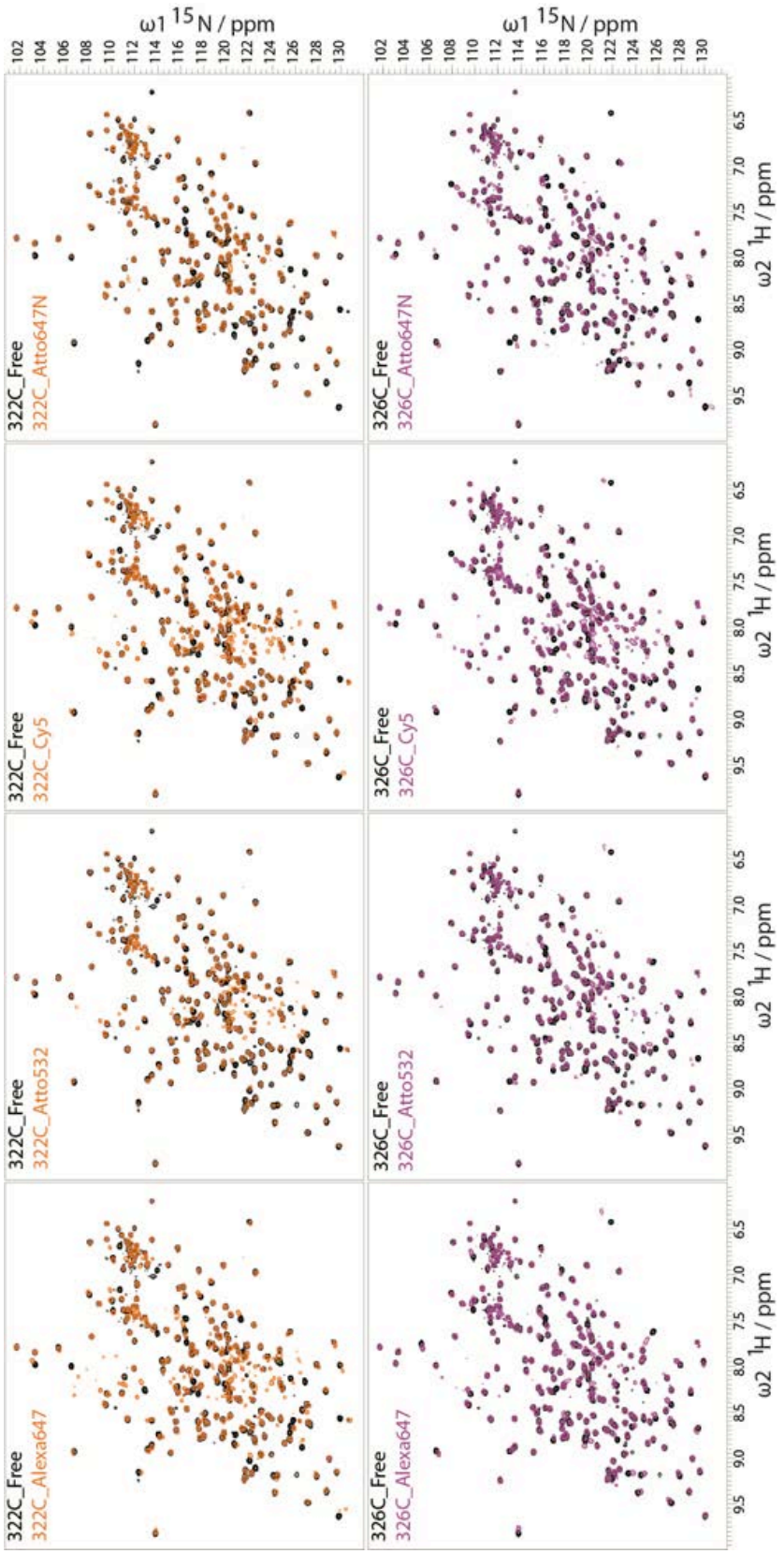

Supplementary Figure S6: **The effect of the donor fluorophore Atto532 and the acceptor fluorophores Alexa647, Cy5, and Atto647N at positions C322 and C326 on the conformation of U2AF65 (RRM1,2) studied by NMR.** Comparison of the $^{1}H,^{15}N$-HSQC spectra of unlabeled RRM1,2 (black) and RRM1,2 labeled with the fluorophores at position C322 (orange) or C326 (magenta).

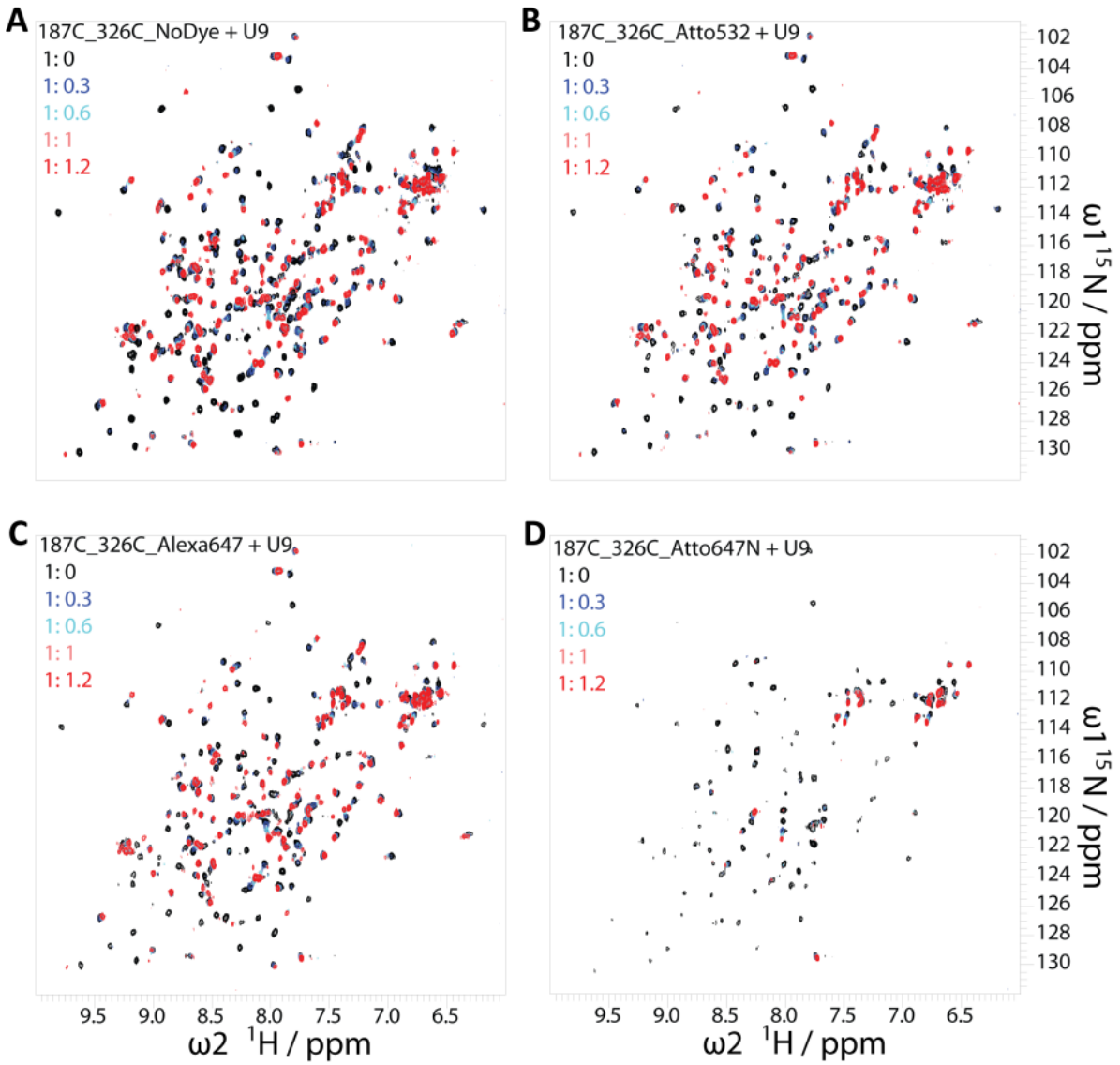

Supplementary Figure S7: **The effect of the fluorophores Atto532, Alexa647, and Atto647N of the dual-position mutant U2AF65(RRM1,2)-C187/C326 on RNA binding studied by NMR.** Comparison of the ^{1}H,^{15}N-HSQC spectra of RRM1,2 upon titration with U9 RNA. **(A)** unlabeled RRM1,2. **(B)** RRM1,2-C187-C326-Atto532. **(C)** RRM1,2-C187-C326-Alexa647. **(D)** RRM1,2-C187-C326-Atto647N. Note, that the highly aromatic Atto647N dye causes substantial line-broadening in the presence of RNA, presumably by a combination of effects on the protein conformation and potential interactions with the RNA bases.

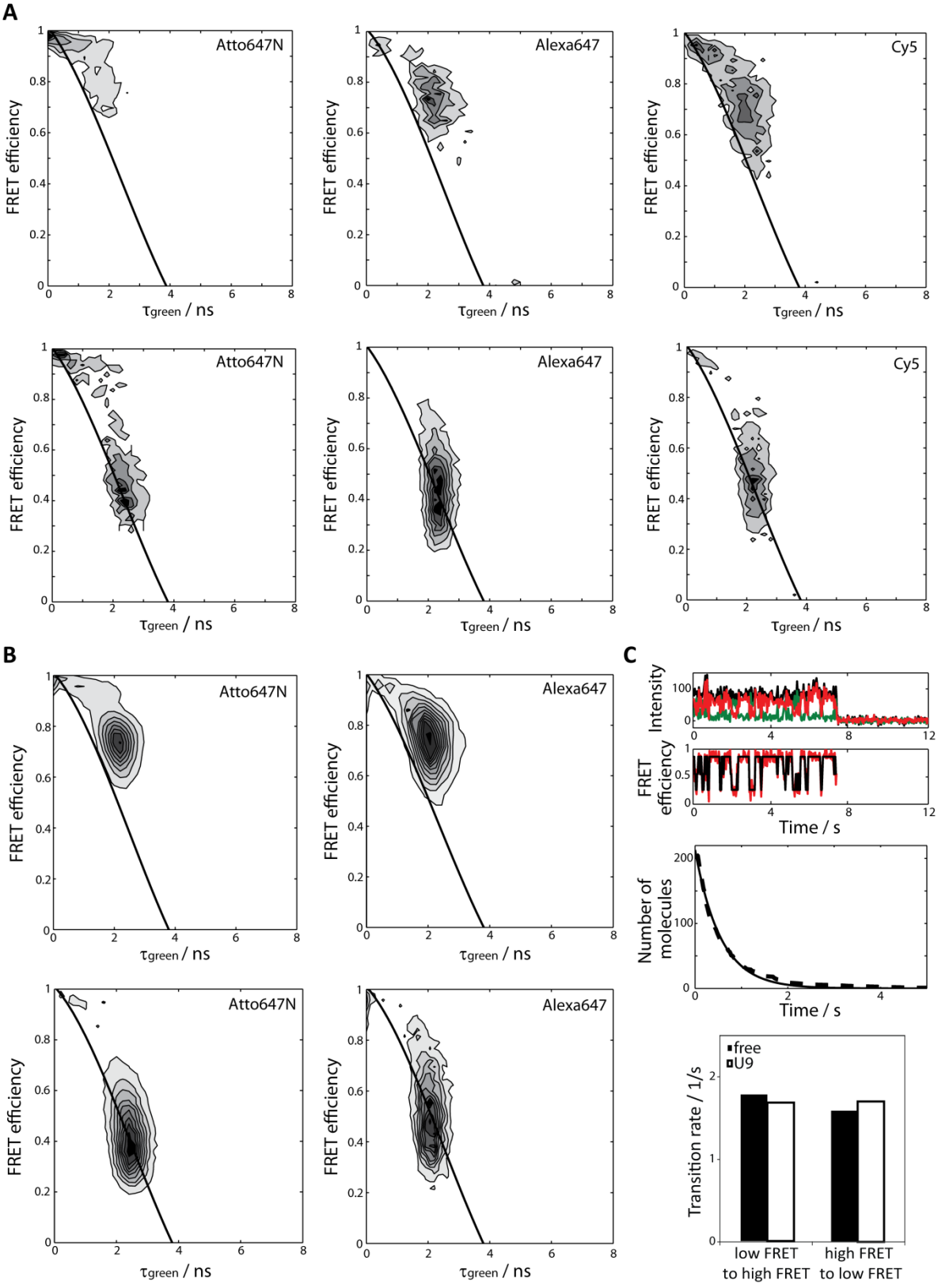

Supplementary Figure S8: **Effect of the acceptor fluorophore on the observation of conformational dynamics in U2AF65 constructs.** (**A**) Histograms of FRET efficiency versus donor lifetime of RRM1,2-C187-C318 labeled with Atto532 and the different acceptor fluorophores Atto647N (*left*), Alexa647 (*middle*), and Cy5 (*right*) in the absence of RNA (*upper panels*) and when bound to U9 RNA (*lower panels*). (**B**) Histograms of FRET efficiency versus donor lifetime of RRM1,2-C187-C326 labeled with Atto532 and the

acceptor fluorophores Atto647N (*left*) and Alexa647 (*right*) in the absence (*upper panels*) and presence (*lower panels*) of U9 RNA. (**C**) Conformational dynamics of RRM1,2-C187-C318-Atto532/Atto647N encapsulated in lipid vesicles and immobilized on the surface observed by TIRF microscopy. Exemplary intensity time trace of a dynamic RRM1,2 molecule (*upper panel*) with the intensity of the donor shown in green, the acceptor intensity in red, and the total intensity in black. Exemplary survival time of RRM1,2 molecules in the low FRET state fit by a single exponential decay (*middle panel*). Switching rates of RRM1,2 from the low FRET to the high FRET state as well as from the high FRET to the low FRET state in the absence and presence of U9 RNA.